11th World Congress on Computational Mechanics (WCCM XI)
5th European Conference on Computational Mechanics (ECCM V)
6th European Conference on Computational Fluid Dynamics (ECFD VI)
E. Oñate, J. Oliver and A. Huerta (Eds)

TOWARDS FIBER BUNDLE MODELS FOR COMPOSITE PRESSURE VESSELS

Jörg B. Multhoff

ISATEC GmbH, Rathausstr. 10, 52072 Aachen, Germany
j.multhoff@isatec-aachen.de, www.isatec-aachen.de

Key words: Composite Pressure Vessel, Filament Winding, Fiber Bundle Model

Abstract. Finite element models for composite pressure vessels (CPV) are usually based on the classical laminate theory (CLT). In the CLT the composite laminate is represented by a stack of homogeneous plies. Each ply is described by thickness, orientation angle and orthotropic mechanical properties. For filament wound CPV each layer is frequently modeled by two unidirectional plies with opposite fiber angles. Ply thickness and fiber angle vary throughout the laminate depending on vessel geometry and fiber path. The thickness build-up due to overlap is described by analytical or semi-empirical formulas. Close observation of the actual fiber geometry of filament wound CPV reveals that this model is only a simplification of reality. Because of the finite band width and band overlap more than two plies may be present at any point of the wound layer. The fiber angle at a given point is not unique in the actual ply stack. These effects can be modeled by an enhanced filament winding simulation which tracks the deposition of a finite-width band on the winding surface. However, the transformation of this detailed laminate information into a suitable finite element model based on CLT is not well-defined. The classical approach uses layered shell or solid elements to model the laminate. This requires the use of a certain number of plies, each with unique angle and thickness within every finite element. A mesh layout which respects the detailed description of the real laminate within the framework of CLT is hard to envision. In the present research the filament wound band is modeled as a group of fiber bundles following the real fiber path on the winding surface. The fiber bundles are embedded in a structured mesh representing the matrix material. The fiber bundle approach may be the appropriate bridge between micro and macro descriptions of the composite materials resulting from filament winding. In this contribution the main idea of the fiber bundle approach is motivated, explored and compared with modeling strategies based on layered solid elements. The fiber bundle approach may be extended to filament wound, fiber-placed or braided structures with partial surface coverage which are even more difficult to describe by CLT. Applications are in the safe and economic design of high pressure hydrogen tanks for automotive applications.

1 INTRODUCTION

The interest in gas storage for mobile applications is steadily growing. This leads to a rising demand for light-weight composite pressure vessels. However, the behavior of composite structures is unintuitive and not easy to predict. The safe and efficient design of composite pressure vessels therefore requires thorough analysis [1].

Important features of composite materials and filament winding are described briefly to give the necessary background for the discussion of finite element analysis methods for composite pressure vessels (CPV) and to motivate the present work.

1.1 Fibrous Composite Materials

Structural composites are generally defined as materials consisting of two or more phases on a macroscopic scale, whose mechanical performance are designed to be superior to those of the constituent materials acting independently [2]. In particular, fiber-reinforced plastic materials consist of stiff and strong fibers embedded in a soft matrix material. Material in fiber form exhibits the highest tensile strength of all material forms. However, the strength of the fiber is reduced with increased length due to the higher probability of a local weakness. Embedding a multitude of parallel fibers at high volume fraction in a soft matrix material enables them to share loads and to mitigate the consequences of local failure, among other benefits.

It is important to note that this unidirectional fiber-reinforced composite material has excellent stiffness and strength properties only in fiber direction, Tab. 1 and Tab. 2. In general it is necessary to combine multiple layers of unidirectional material with different fiber directions in a laminate to accommodate all loads acting on a structure. The resulting laminate properties usually still show a high directional dependency. Recognizing that the matrix dominated strength properties are much less certain and reproducible than the strength in fiber direction, it is clear that the design should generally not depend on them strongly. Realizing the benefits of fiber-reinforced composite materials for structural application requires a considerably higher analysis effort than the use of traditional structural materials.

Table 1: Illustrative unidirectional CFRP elastic properties (in-plane) [3]

Description	Symbol	Value
Parallel Modulus	E_1	171.4 GPa
Transverse Modulus	E_2	9.08 GPa
Shear Modulus	G_{12}	5.29 GPa
Major Poisson's Ratio	ν_{12}	0.32

Table 2: Illustrative unidirectional CFRP strength properties (in-plane) [3]

Description	Symbol	Value
Parallel tensile strength	R_1^+	2326.2 MPa
Parallel compressive strength	R_1^-	1200.1 MPa
Transverse tensile strength	R_2^+	62.3 MPa
Transverse compressive strength	R_2^-	199.8 MPa
Shear strength	R_6	92.3 MPa

1.2 Filament Winding

Filament winding is one of the oldest manufacturing methods for structural composites [4]. Wet winding has the advantages of using the raw materials, fiber and resin, in its direct form without intermediate processing steps. The manufacturing speed measured in mass per time is among the highest in comparison to other methods. In sum, this contributes to relatively low manufacturing costs for filament wound composite materials compared to other methods [5] and explains its continued importance.

In the filament winding process multiple rowings or tows, each composed of thousands of fibers, are formed to a flat band and are impregnated with a matrix material, usually a resin. A typical fiber volume fraction V_f is 60%. The band is continuously deposited on a rotating mandrel, eventually covering the entire surface. The resulting winding pattern consists of multiple cycles, in each cycle the band follows a specific path along the winding surface, Fig. 1. This path is characterized by a certain angle α of the band and thus the fibers relative to the *meridian* of the winding surface. Usually the cylindrical part of the vessel is covered in such a way that the resulting layer is composed of two bands with opposing fiber angles $(+\alpha/-\alpha)$ at each location.

Notable characteristics of the filament wound structure are the distribution of the winding angle and the layer thickness along the winding surface. The details depend on the winding pattern. Usually winding angle and thickness are constant in the cylindrical part of the vessel (α_0, t_0).

1.3 Analysis of Composite Pressure Vessels

Different analysis methods are available and in use for composite pressure vessels [6]. All have to take into account the special features arising in the filament wound composite structure as described before. Netting analysis deserves special mention as the first analysis method for composite pressure vessels, introducing the important concept and design principle that the fiber network takes all the loads [5]. However, only finite element analysis has the potential to model all relevant effects. A review of finite element analysis methods for filament wound composite pressure vessels was given in [7].

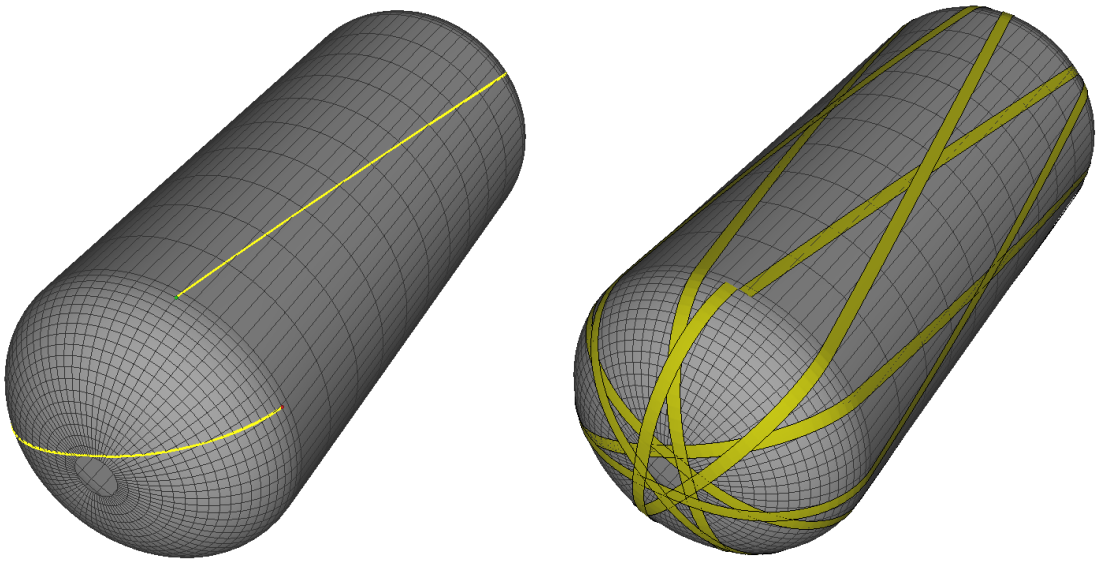

Figure 1: Fiber path (left) and unidirectional band (right) on the winding surface.

2 FILAMENT WINDING SIMULATION

The effects of the filament winding process on the resulting fiber architecture is not self-evident and requires analysis by filament winding simulation.

2.1 Fiber Path

The wet fiber can be deposited on the surface only on – or close to – a geodesic path without slipping. On a surface of revolution with local radius r the geodesic path is given by Clairaut's theorem [4, 5]: $r\sin(\alpha) = \text{const}$. The fiber is tangent at the polar opening with radius r_p, i.e. $\alpha(r_p) = 90°$. These layers are called helical layers. For geodetic winding the fiber angle at each radius can be evaluated by Eqn. (1). Figure 2 shows an example for this fiber angle distribution. Some deviation from this path is possible if the surface friction or material adhesion is exploited.

$$\alpha(r) = \arcsin\left(\frac{r_p}{r}\right) \tag{1}$$

Layers with a constant winding angle close to 90° are called hoop layers and can only be applied in the cylindrical part of the vessel. The polar opening radius of these layers is equal to or close to the radius in the cylindrical part of the vessel. Practical designs require multiple helical and hoop layers each with different winding angle α_0 and corresponding polar opening diameters.

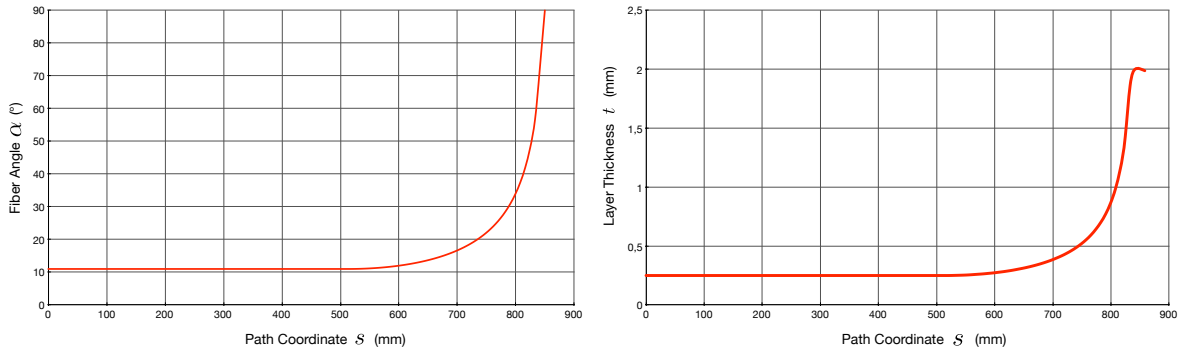

Figure 2: Example for fiber angle (left) and thickness distribution (right).

2.2 Layer Thickness

One feature of the continuos filament winding process is that each *parallel* of the winding surface is crossed by the same number of fibers. This results in a constant layer thickness in the cylindrical part of the vessel. However, the layer thickness increases with decreasing vessel radius. This is a consequence of the progressive band overlap that can be easily recognized in Fig. 1 and Fig. 3. The resulting layer thickness distribution is shown in Fig. 2. This behavior can be approximately described by Eqn. (2) up to a certain distance from the polar opening.

$$t(r) = t_0 \frac{r_0 \ \cos(\alpha_0)}{r \ \cos(\alpha)} \tag{2}$$

Improved prediction of the layer thickness is possible by empirical or analytical methods [6] and by the enhanced filament winding simulation.

2.3 Enhanced Filament Winding Simulation

The main differences between the real fiber architecture of filament wound vessels and the idealized theory as described above can be recognized by explicit consideration of the finite fiber band width w in an enhanced version of the filament winding simulation.

After computing the fiber path, the geometry of the fiber band, usually consisting of multiple parallel fiber strands, is modeled, Fig 1. The fiber band is represented by patches of triangles connecting consecutive bounding points. The local thickness is computed by accumulation of band patches at sampling points on the winding surface. Likewise the local laminate stacking sequence at any sampling point can be computed. Details are presented in [8].

2.4 Local Laminate Properties

The main results of the simulated band deposition on the winding surface are consistent with observations that can also be made with actual vessels manufactured by filament

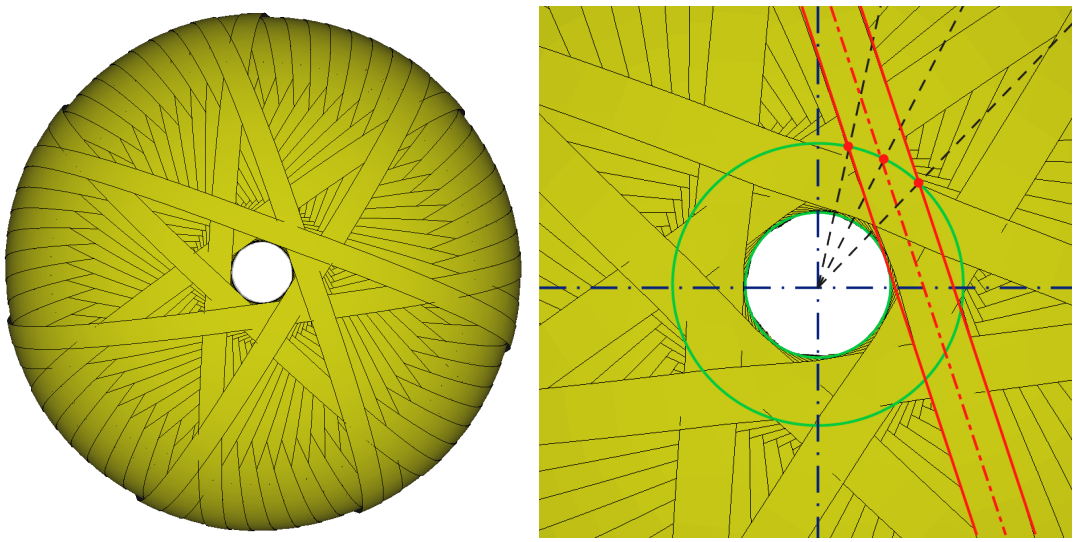

Figure 3: Overlap of the unidirectional band in the dome (left) and near the polar opening (right).

winding. The differences between the real laminate structure and the idealized theory are mainly due to the finite width w of the filament band. They are reduced with decreasing width of the band. Additional differences may exist due to fiber bridging effects.

The main observations are:

1. The effective thickness distribution along the meridian direction is not continuos as in Fig. 2 but stepped due to the band overlap.

2. The thickness at a given meridian position in circumferential direction is not constant but variable and depends on the winding pattern.

3. The local fiber angle within a layer at a given meridian and circumferential position is not constant in the circumferential direction (Fig. 3) and is in general not given by Clairaut's theorem as shown in Fig. 2

In sum the important local properties fiber angle and layer thickness possess a discontinuous distribution in the laminate. For optimized composite pressure vessel designs it is of high interest to examine the effects of these observations on the structural behavior.

2.5 Representation of Local Properties in the Analysis Model

The transfer of the laminate data generated by the enhanced filament winding simulation into the finite element model may proceed as follows: In the simplest case, the grid points representing the winding surface are used as nodal points of the finite element discretization. The finite elements may be shell or solid elements. However, only solid elements allow for the required detailed analysis. In the case of solid elements the grid

points represent the nodes on the inner surface and the nodes on the outside surface are generated using the normal vectors of the winding surface and the thickness data. The required thickness information for each node is taken from the accumulated band thickness at the nodal points. Depending on the element type, the internal laminate description may allow for multiple layers with constant thickness and constant angle of principle material direction or for variable thickness layers with variable angle of principle material direction. In the latter case, the thickness and angle data usually have to be input at the nodal points. However, most finite element formulations require that the layers are continuous within the element and thus that the number of layers is the same at all nodes.

It turns out that this may not be the case for general filament wound structures. The easiest solution to this problem is to use a sampling point in the center of the element to record the local laminate stacking sequence and to use this data to define the laminate corresponding to the entire element. This may represent the real stiffness and strength distribution poorly. A more accurate approach may be to use the location of the in-plane integration points of the element as the sampling points, e.g. for 4 x 4 in-plane Gauss integration. Different laminate stacking sequences with individual number of layers would result at the in-plane integration points, making special element formulations necessary.

A mesh layout which respects the detailed description of the real laminate as shown e.g. in Fig. 3 within the framework of a laminate theory is hard to envision.

To avoid the mentioned problems, in the present research the filament wound band is modeled as a group of fiber bundles following the real fiber path on the winding surface. The fiber bundles are embedded in a structured mesh representing the matrix material.

3 FINITE ELEMENTS FOR FILAMENT WOUND STRUCTURES

The finite element analysis of composite laminates based on the assumptions of the classical laminate theory is described e.g. in [9]. The most appropriate representation, especially for thick-walled vessels, can be achieved using layered solid elements. In general multiple elements in thickness direction are necessary [7]. Shell elements are beyond the scope of this discussion.

3.1 Layered Solid Element

The concept of the layered solid element is reviewed in two versions for constant and for variable layer thickness. Aspects of geometric nonlinearity and element technology are neglected for simplicity. Only the formulation of the element stiffness matrix is considered. The notation of the original sources is preserved.

3.1.1 Constant Layer Thickness

One example for the formulation of the layered solid element for constant thickness layers is proposed in [10]. Using the isoparametric concept the stiffness matrix $[KF]$ can be evaluated by Eqn. (3) in terms of the strain interpolation matrix $[BF]$, the constitutive

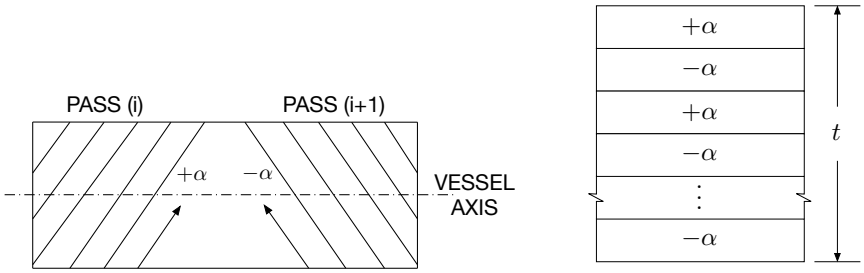

Figure 4: Representation of filament wound composite pressure vessel wall using CLT [10].

matrix $[EI']$ and the Jacobian matrix $[J]$ in the standard way [11].

$$[KF] = \int_{-1}^{+1} \int_{-1}^{+1} \int_{-1}^{+1} [BF]^T [EI'][BF] \det[J] \; d\xi \, d\eta \, d\zeta \tag{3}$$

The integral can be evaluated by numerical integration. However, the constitutive matrix $[EI']$ is not continuous in the element but is different from layer to layer due to the necessary transformation from the principle directions of the orthotropic material to the global coordinate directions. This is handled by splitting the integration limits through each layer. For the application of the Gauss quadrature formula the integration limits within each layer should be from -1 to $+1$. This is achieved by a change of variable for the thickness coordinate ζ as formulated in Eqn. (4).

$$\zeta = -1 + \frac{1}{t} \left[-h_k(1 - \zeta_k) + 2 \sum_{j=1}^{k} h_j \right] \tag{4}$$

Using this equation the thickness coordinate ζ_k in layer k varies from -1 to $+1$ and the change of variables involves effectively a scaling factor for the layer thickness h_k relative to the total element thickness t:

$$d\zeta = \left(\frac{h_k}{t} \right) d\zeta_k \tag{5}$$

With this substitution for $d\zeta$ the stiffness matrix in Eq. (3) can be evaluated as the sum over all n layers contained in the element.

$$[KF] = \sum_{k=1}^{n} \int_{-1}^{+1} \int_{-1}^{+1} \int_{-1}^{+1} [BF]^T [EI'][BF] \det[J] \frac{h_k}{t} \; d\xi \, d\eta \, d\zeta_k \tag{6}$$

This formulation illustrates the idea of the layered solid element very well but is of limited applicability for filament wound structures with variable layer thickness.

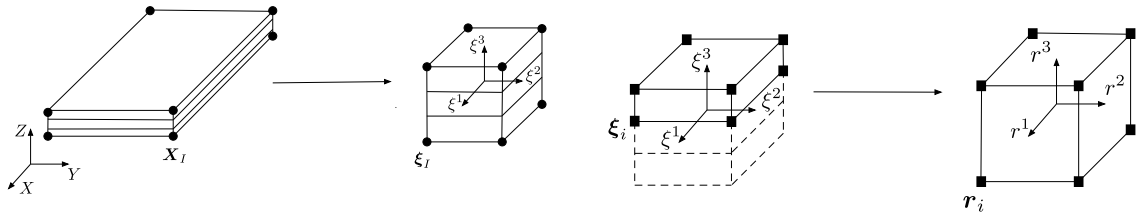

Figure 5: First and second isoparametric map for integration of layered elements [12].

3.1.2 Variable Layer Thickness

An element formulation allowing for variable element thickness – among other features – is proposed in [12]. Here only the integration scheme for the linear stiffness matrix is considered. The element geometry is interpolated with tri-linear shape functions. After the first isoparametric map a second isoparametric map for each layer is introduced, Fig. 5. The coordinates $\boldsymbol{\xi} = [\xi^1, \xi^2, \xi^3]^T$ of the first map are interpolated in terms of the coordinates $\boldsymbol{r} = [r^1, r^2, r^3]^T$ of the second map using Eqn. (7) and (8). $\boldsymbol{\xi_i}$ contains the coordinates of the layer under consideration.

$$\boldsymbol{\xi} = \sum_{i=1}^{nnode} \bar{N}_i \boldsymbol{\xi_i} \tag{7}$$

$$\bar{N}_i = \frac{1}{8}(1 + r^1 r_i^1)(1 + r^2 r_i^2)(1 + r^3 r_i^3) \tag{8}$$

The components of the element stiffness matrix $\boldsymbol{K}_{eIJ}$ are evaluated by summation over all layers $nlay$ and over all integration points $ngaus$:

$$\boldsymbol{K}_{eIJ} = \sum_{L=1}^{nlay} \sum_{gp=1}^{ngaus} \boldsymbol{B}_I^T(\boldsymbol{\xi}_{gp}^L) \mathbb{C}_L \boldsymbol{B}_J(\boldsymbol{\xi}_{gp}^L) \det \boldsymbol{J}(\boldsymbol{\xi}_{gp}^L) \det \boldsymbol{J}^L(\boldsymbol{r}_{gp}^L) w_{gp}^L \tag{9}$$

Here, $\boldsymbol{J}$ and $\boldsymbol{J}^L$ are the Jacobian matrix of the first and second map and w_{gp}^L are the weighting factors of the integration point. $\boldsymbol{B}$ is the strain interpolation matrix and $\mathbb{C}_L$ is the constitutive matrix in layer L.

For the modeling of a filament wound structure with a stack of layered solid elements with variable layer thickness the total laminate must be mapped on the laminate pertaining to the individual elements.

3.2 Reinforcing Element

The application of truss elements embedded in solid elements for the modeling of dry filament wound pressure vessels was proposed in [13]. This can be realized by constraining the nodal degrees of freedom of the truss element to the degrees of freedom of the

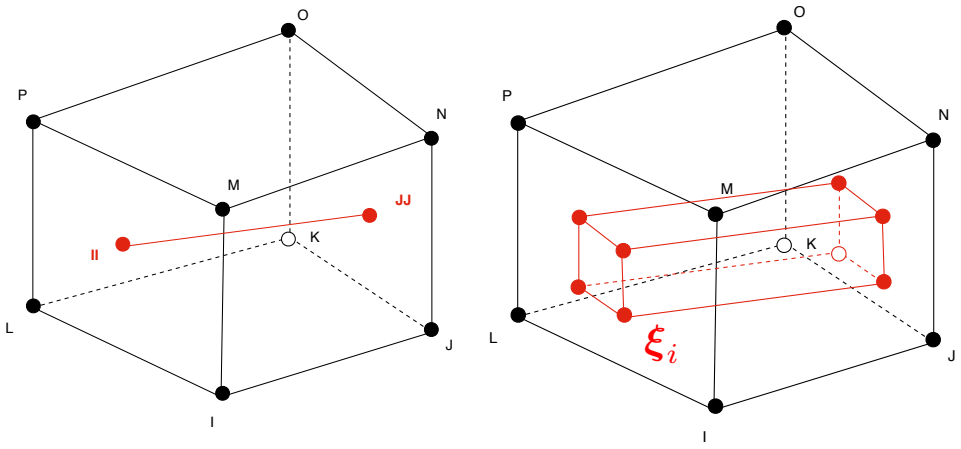

Figure 6: Reinforcing element embedded in a solid element (left). Fiber bundle element (right).

embedding solid element. Thus the displacement field of the solid element imposes the displacements of all embedded truss elements.

The same effect can be achieved by classical reinforcing elements as described e.g. in [14]. Here, the degrees of freedom of the reinforcing element $\{u_{II}, v_{JJ}, w_{II}\}^T$ are expressed in terms of the degrees of freedom of the embedding element $\{u_i, v_i, w_i\}^T$ by way of the eight tri-linear shape functions of the embedding element N_i by Eqn. (10), Fig. 6.

$$\begin{Bmatrix} u_{II} \\ v_{II} \\ w_{II} \end{Bmatrix} = \sum_{i=1}^{8} N_i(\xi_{II}, \eta_{II}, \zeta_{II}) \begin{Bmatrix} u_i \\ v_i \\ w_i \end{Bmatrix} \tag{10}$$

Using this transformation the stiffness matrix of the reinforcing element can be expressed in terms of the degrees of freedom of the embedding element and superimposed to form the total stiffness. Typically, the reinforcing element allows the definition of multiple reinforcing members. This formulation is restricted to unidirectional reinforcement in the direction of the reinforcing members. This may be appropriate for the modeling of dry filament wound structures without use of matrix materials or for analysis on the basis of the assumption of netting analysis.

For the modeling of a filament wound structure the global fiber architecture must be mapped on the reinforcing members in the individual elements.

3.3 Fiber Bundle Element

The idea of the fiber bundle element is to form a synthesis of the layered element and the reinforcing element as a practical meso-level model for the fiber architectures arising from filament winding.

In a first variant the geometry of each fiber bundle is modeled by a prismatic shape that can be mapped on a cube. This variant is similar to the layered element with

variable layer thickness as described before but has a generalized geometry of the second isoparametric map, Fig. 6. $\boldsymbol{\xi_i}$ in Eqn. (7) now contains the coordinates of the fiber bundle under consideration. This variant of the fiber bundle element may use the same Gauss integration formula as the layered element.

In a second variant each fiber bundle is modeled by a volume simply computed from length and cross section area. This variant is similar to the reinforcing element described before but allows the alternative use of a one-dimensional or a three-dimensional constitutive model. In the latter case the reinforcement is not purely unidirectional. This variant could use a one-point integration rule.

The components of the element stiffness matrix for both variants are evaluated as follows:

$$\boldsymbol{K}_{eIJ} = \sum_{B=1}^{nbundle} \sum_{ip=1}^{nip} \boldsymbol{B}_I^T(\boldsymbol{\xi}_{ip}^B) \mathbb{C}_B \boldsymbol{B}_J(\boldsymbol{\xi}_{ip}^B) \det \boldsymbol{J}(\boldsymbol{\xi}_{ip}^B) \det \boldsymbol{J}^B(\boldsymbol{r}_{ip}^B) w_{ip}^B \tag{11}$$

The differences between the to variants are the number of integration points, the effective formulas for the Jacobian matrix of the second isoparametric map $\boldsymbol{J}^B$ and the weighting factor w_{ip}^B of the integration points. $\mathbb{C}_B$ is the constitutive matrix for the fiber bundle B.

The first variant may be more costly than the second variant due to the higher number of integration points. However, evaluation of the relative efficiency is subject to verification of the element behavior.

4 CONCLUSIONS

The enhanced filament winding simulation confirms the observation that filament wound composite pressure vessel structures possess discontinuous fiber angle and layer thickness distributions. This poses difficulties for the accurate modeling using layered elements based on the assumptions of the classical laminate theory. Consideration of the implementation of layered solid elements and reinforcing elements motivates the formulation of a fiber bundle element that may be more effective for the analysis of filament wound structures. Implementation of this concept is proceeding and requires further work in the infrastructure of the enhanced filament winding simulation and in testing of the fiber bundle element. The fiber bundle approach may be the appropriate bridge between micro and macro descriptions of the composite materials resulting from filament winding and may be extended to structures arising from fiber placement and braiding processes. The results are relevant for the safe and economic design of optimized high pressure hydrogen tanks for automotive applications.

REFERENCES

[1] J.B. Multhoff, J. Krieger. Effective Structural Design Procedure for Composite Hydrogen Tanks. *18th World Hydrogen Energy Conference 2010*, Essen, Germany, 2010

[2] I.M. Daniel and O.I. Ishai. *Engineering Mechanics of Composite Materials*. Oxford University Press, 1994

[3] E.J. Barbero. *Introduction to Composite Materials Design*. 2nd Edition. CRC Press, 2011

[4] D.C. Rosato and C.S. Grove. *Filament Winding: Its development, manufacturing, application, and design*. John Wiley & Sons, 1964

[5] S.T. Peters, W.D. Humphrey and R.F. Foral. *Filament Winding Composite Structure Fabrication*. 2nd Edition. SAMPE Publishers, 1999.

[6] V.V. Vasiliev. *Composite Pressure Vessels: Design, Analysis and Manufacturing*. Bull Ridge, 2009

[7] J.B. Multhoff, J. Krieger, L.E.V. Loures da Costa and J. Betten. Problems in High-Resolution Finite Element Models of Composite Rocket Motor Cases". *Proceedings of COBEM 2001*, Uberlândia, Vol. **6**, 207–216, 2001

[8] J.B. Multhoff. Enhanced Filament Winding Simulation for Improved Structural Analysis of Composite Pressure Vessels. *The 19th International Conference on Composite Materials*, Montreal, 2013

[9] O.O. Ochoa and J.N. Reddy. *Finite Element Analysis of Composite Laminates*. Kluwer Academic Publishers, 1992.

[10] S.V. Hoa, C.W. Yu and T.S. Sankar. Analysis of Filament Wound Vessel Using Finite Elements. *Composite Structures*, Vol. **3**, 1–18, 1985.

[11] O.C. Zienkiewicz and R.L. Taylor. *The finite element method*. 6th Edition. Elsevier, 2005

[12] S. Klinkel, F. Gruttmann and W. Wagner. A continuum based three-dimensional shell element for laminated structures. *Computers and Structures*, Vol. **71**, 43–62, 1999

[13] J.J. Koppert, H. de Boer, A.P.D. Weustink, A. Beukers and H.E.N. Bersee. Virtual Testing of Dry Filament Wound Thick Walled Pressure Vessels. *The 16th International Conference on Composite Materials*, Kyoto, 2007

[14] G. Hofstetter and H.A. Mang. *Computational Mechanics of Reinforced Concrete Structures*. Vieweg, 1995